HHS Public Access

Author manuscript

Auton Neurosci. Author manuscript; available in PMC 2017 July 25.

Published in final edited form as:

Auton Neurosci. 2016 July ; 198: 38–49. doi:10.1016/j.autneu.2016.07.007.

δ-opioid receptors: pivotal role in intermittent hypoxia-augmentation of cardiac parasympathetic control and plasticity

Juan A. Estrada, **Mathew A. Barlow***, **Darice Yoshishige**, **Arthur G. Williams Jr.**, **H. Fred Downey**, **Robert T. Mallet**, and **James L. Caffrey**

Institute of Cardiovascular and Metabolic Diseases, University of North Texas Health Science Center, Fort Worth, TX, USA

*Department of Biology, Eastern New Mexico University, Portales, NM, USA

Abstract

Background—Intermittent hypoxia training (IHT) produces robust myocardial protection against ischemia-reperfusion induced infarction and arrhythmias. Blockade of this cardioprotection by antagonism of either β_1-adrenergic or δ-opioid receptors (δ-OR) suggests autonomic and/or opioidergic adaptations.

Purpose—To test the hypothesis that IHT shifts cardiac autonomic balance toward greater cholinergic and opioidergic influence.

Methods—Mongrel dogs completed 20 d IHT, non-hypoxic sham training, or IHT with the δ-OR antagonist naltrindole (200 μg/kg *sc*). The vagolytic effect of the δ-OR agonist met-enkephalin-arg-phe delivered by sinoatrial microdialysis was evaluated following IHT. Sinoatrial, atrial and left ventricular biopsies were analyzed for changes in δ-OR, the neurotrophic monosialoganglioside, GM-1, and cholinergic and adrenergic markers.

Results—IHT enhanced vagal bradycardia *vs.* sham dogs ($P<0.05$), and blunted the δ_2-OR mediated vagolytic effect of met-enkephalin-arg-phe. The GM- 1 labeled fibers overlapped strongly with cholinergic markers, and IHT increased the intensity of both signals ($P<0.05$). IHT increased low and high intensity vesicular acetylcholine transporter labeling of sinoatrial nodal fibers ($P<0.05$) suggesting an increase in parasympathetic arborization. IHT reduced select δ-OR labeled fibers in both the atria and sinoatrial node ($P<0.05$) consistent with moderation of the

Correspondence: Robert T. Mallet, Ph.D., Institute of Cardiovascular and Metabolic Diseases, University of North Texas Health Science Center, 3500 Camp Bowie Boulevard, Fort Worth, TX 76107-2699 USA, Telephone: 817-735-2260, Robert.Mallet@unthsc.edu.

5.0 Conflicts of Interest and Ethical Standards

No conflicts of interest, financial or otherwise, are declared by the authors. Experimentation on animals was conducted in accordance with the *Guide to the Care and Use of Laboratory Animals* (U.S. National Research Council Publication 85–23, revised 2011). Approval for testing on animals was obtained through the Institutional Animal Care and Use Committee of the University of North Texas Health Science Center at Fort Worth. This work was supported by research grants AT-003598 from the U.S. National Institutes of Health, and 03-04-49065 from the University of North Texas Health Science Center (UNTHSC). JAE was supported by a predoctoral fellowship from UNTHSC Graduate School of Biomedical Sciences' *Minority Opportunities in Research and Education* program.

vagolytic δ_2-OR signaling described above. Furthermore, blockade of δ-OR signaling with naltrindole during IHT increased the protein content of δ-OR (atria and ventricle) and vesicular acetylcholine transporter (atria) *vs.* sham and untreated IHT groups. IHT also reduced the sympathetic marker, tyrosine hydroxylase in ventricle ($P<0.05$).

Summary—IHT shifts cardiac autonomic balance in favor of parasympathetic control via adaptations in opioidergic, ganglioside, and adrenergic systems.

Keywords

acetylcholine; enkephalin; GM-1; naltrindole; vagus

1. INTRODUCTION

Controlled IHT reduces cardiac arrhythmias and improves the clinical efficacy of pharmacological agents [Manukhina et al., 2006]. IHT also dramatically increases myocardial resistance to ischemia-reperfusion injury and arrythmogenesis in dogs [Zong et al., 2004; Mallet et al., 2006; Estrada et al., 2016] and rats [Manukhina et al., 2013], and preserves post-infarct vascular endothelial responses and coronary blood flow in rats [Manukhina et al., 2013]. This gradually evolving, IHT mediated cardioprotection is abrogated by antioxidants or antagonists of β_1-adrenergic (β_1-AR) or δ-opioid (δ-OR) receptors [Mallet et al., 2006; Estrada et al., 2016]. Collectively, these findings indicate that IHT mobilizes adrenergic, opioid and reactive oxygen species (ROS) signaling systems, to induce a unique ischemia resistant phenotype. Consistent with these observations, hypoxic training elicits enkephalin accumulation in myocardium [Maslov et al., 2013].

Acute hypoxia appears to improve cholinergic transmission in both adrenergic and opioid environments [Levy & Zieske 1969; Farias et al 2003]. For example, when enkephalins accumulate locally during repeated coronary occlusions, vagal transmission improves [Jackson et al., 2001]. This improved vagal function appears to result from a shift in the local receptor environment that favors the vagotonic δ_1-OR [Farias et al., 2001] at the expense of vagolytic δ_2-ORs. The environmental shift may result from local changes in the vagotonic neurotropin monosialoganglioside-1 (GM-1) [Davis et al., 2006].

The δ-OR is widely expressed on parasympathetic fibers innervating atrial and sinoatrial tissues [Deo et al., 2008], and stimulation of δ-ORs induces GM-1 synthesis and nerve growth [Narita et al., 2006, Kappagantula et al., 2014]. The net result is more efficient vagotonic δ_1-OR signaling and parasympathetic transmission [Ledeen and Wu, 2015]. The resulting hypothesis suggests that IHT should improve parasympathetic influence by producing greater arborization and selected increases in GM-1, δ-OR, cholinergic markers and reciprocal declines in adrenergic markers. This study was designed to evaluate functional, biochemical and structural evidence in support of this hypothesis.

2. MATERIALS AND METHODS

2.1 Animals

All animal experimentation was approved by the Institutional Animal Care and Use Committee of the University of North Texas Health Science Center and conducted in accordance with the *Guide to the Care and Use of Laboratory Animals* (U.S. National Research Council Publication 85–23, revised 2011). Mongrel dogs were assigned to 3 groups: non-hypoxic sham (n= 6), IHT (n= 11), or IHT + daily *sc* naltrindole (IHT + N; n= 2). Dogs completed a previously described IHT program [Zong et al., 2004; Estrada et al., 2016] consisting of 20 consecutive days of 5–8 daily cycles of 5–10 min hypoxia (9.5–10% FIO_2) and 4 min intervening room air exposures in a 270 l acrylic chamber [Zong et al., 2004]. The IHT + N dogs received the δ-OR antagonist naltrindole 15 min before each hypoxia session. Naltrindole hydrochloride (Sigma-Aldrich, St. Louis, MO, USA) was dissolved (2 mg/ml) in sterile 0.9% NaCl, filtered and injected (200 μg/kg, *sc*) as described previously [Estrada et al., 2016]. Sham dogs were exposed to 21% O_2 for 20 consecutive days [Zong et al., 2004; Mallet et al., 2006]. On day 21 animals were physiologically evaluated and cardiac tissue was sampled for biochemical and histochemical analyses.

2.1.1 Surgical preparation and instrumentation—Surgical preparation was performed as previously described [Farias et al., 2003]. Briefly, sodium pentobarbital (32.5 mg/kg, *iv*) anesthetized dogs were intubated and ventilated mechanically with room air at approximately 225 mL/kg/min. Supplemental pentobarbital was administered as required. An infusion port Millar Mikro-Tip transducer was inserted into the right femoral artery and advanced into the aorta above the L5 region to measure heart rate and sample arterial blood, and to perfuse the target L5 sympathetic ganglion with experimental agents. Lead II electrocardiogram was continuously monitored via surface electrodes. An electro-magnetic flow probe (10 mm) was installed around the left femoral artery to measure hindlimb blood flow. Blood gases, bicarbonate concentration and pH in arterial samples were measured with an Instrumentation Laboratory Gem Premier 3000 blood gas analyzer (Lexington, MA, USA). The pO_2 (90–120 mmHg), pH (7.35–7.45), and pCO_2 (30–40 mmHg) were kept within the respective normal limits by administering supplemental O_2 or bicarbonate, or by adjusting the minute ventilation. The right and left cervical vagus nerves were isolated through a ventral midline incision and double ligated with umbilical tape to abort afferent nerve traffic. The nerves were then returned to the prevertebral compartment for later retrieval. The heart was exposed by right lateral thoracotomy and pericardiotomy. Figure 1 summarizes experimental and analytical procedures applied to the IHT and sham dogs, which are described in the following sections.

2.1.3 Sinoatrial nodal microdialysis—Dialysis probes were made from 1 cm lengths of dialysis fiber (200 μm i.d. × 220 μm o.d.) obtained from a Clirans TAF 08 artificial kidney (Asahi Medical, Northbrook, IL, USA) as previously described [Farias et al., 2003]. Each dialysis probe, with its glass fiber inflow and outflow lines, was inserted into the sinoatrial node using a 25 ga needle. The probe permitted transudation of molecules with masses <36 kDa. A micro infusion pump connected to the inflow line was used to equilibrate the probe with 0.9% NaCl vehicle at 5 μl/min for one hour.

2.1.4 Assessment of vagal bradycardia and vagal δ-OR modulation—Following 1 h post-surgical equilibration, the right vagus nerve was stimulated at a supramaximal voltage (*e.g.*, 15 V) at 3 Hz for 15 s. Heart rate was recorded when it reached a steady state during the stimulus, and then was allowed 105 s for complete post-stimulus recovery. Increasing doses of MEAP ($5{\cdot}10^{-15}$ to $1.5{\cdot}10^{-9}$ mol/min) were then infused by sinoatrial nodal microdialysis and the heart rate response to vagal stimulation was recorded at each MEAP dose. Each new dose was infused for 5 min at 5 μl/min before testing vagal responses. The probe was then perfused with 0.9% NaCl until the baseline vagal response was reconfirmed.

2.1.5 Assessment of gangliolytic δ_2-OR responses on hind limb conductance —Thirty minutes after discontinuing the nodal MEAP, increasing doses of met-enkephalin ($5 \cdot 10^{-8}$ to $1 \cdot 10^{-5}$ mol/kg) were injected into the descending aorta to construct a δ_2-OR dose-response relationship using femoral arterial flow and conductance as the outcome measures. Bolus doses (1 ml) were injected just proximal to the final segmental arteries providing direct access to the L5 sympathetic ganglia controlling femoral conductance [Barlow et al., 2011], and flushed with 5 ml 0.9% saline. The femoral hemodynamic effect of each dose was recorded and allowed to return to baseline for 5–10 min before applying the next dose.

2.2 Biopsy preparation

The heart was stopped by applying 9V current to the epicardium, and biopsies of sinoatrial node, atrium and left ventricle were taken. Biopsies were subdivided; one portion was snap-frozen in liquid N_2 and stored at −80°C, and the other portion was immersion-fixed in 4% paraformaldehyde for 8 h. Fixed tissues were cryoprotected with serial sucrose solutions (10–30%) and then stored at −80°C.

2.3 Protein extraction

Snap-frozen atrial and left ventricular biopsies were pulverized in a liquid N_2-cooled porcelain mortar [von Ziegler et al., 2013] and homogenized in 10 vol (v/w) extraction buffer (1% IGEPAL CA-630, 0.5% cholate, 0.5% SDS, 150 mM NaCl, 10 mM Tris-Cl, 1 mM EDTA, 1 mM PMSF, pH 7.6; Sigma-Aldrich, St. Louis, MO, USA) containing protease and phosphatase inhibitors (Cell Signaling Technology, Danvers, MA, USA) at 4°C. Homogenates were then sequentially drawn through 18, 21 and 23 ga needles to decrease sample viscosity by shearing nucleic acids. Cellular debris was sedimented by 15 min centrifugation (Eppendorf, Hauppage, NY, USA) at 15,000 *g* and 4°C. Total protein concentrations were measured by bicinchoninic acid assay (Pierce Biotechnology, Rockford, IL, USA) in a microplate reader (Bio-Rad, Hercules, CA, USA).

2.4 Protein electrophoresis and immunoblotting

SDS-polyacrylamide (4% *bis*-acrylamide stacking, 10% *bis*-acrylamide resolving) gels (1.0 mm thick) were prepared from stock reagents (Bio-Rad) according to the manufacturer's instructions. Running and transfer buffers were prepared as described [Towbin, 2009] with addition of 0.02% *w/v* SDS to the transfer buffer. Radio-immunoprecipitation assay buffer lysates were combined with concentrated sample loading buffer yielding a mixture

containing 250 mM Tris-HCl, pH 8.5, 2% w/v lithium dodecyl sulphate, 100 mM dithiothreitol, 0.4 mM EDTA, 10% v/v glycerol, 0.2 mM phenol red, 0.2 mM Brilliant Blue G [Cubillos et al., 2010] and 1 mg/mL protein. Samples were heated at 70°C for 10 min, and then cooled on ice. Proteins (5–10 μg/well) were electrophoresed at 60V through the stacking gel and at 100V through the resolving gel, and then electroblotted onto vinyl membranes (Bio-Rad) at 70V for 60–90 min, rinsed with deionized water to remove buffer salts, and dried 1 h at room temperature.

2.5 Immunoblotting, imaging and protein quantification

Membranes were reactivated with a brief rinse in methanol, rehydrated with optimized zwitterionic salt washing buffer (Kirkegaard and Perry, Gaithersburg, MD, USA), and then incubated with blocking buffer (SignaLOCK; Kirkegaard and Perry) for 1 h and with primary antibodies diluted in blocking buffer for 3 h. Membranes were then rinsed 3·5 min in washing buffer, incubated for 1 h with horseradish peroxidase-conjugated secondary antibodies diluted in blocking buffer, and then rinsed 4·5 min in washing buffer and once in deionized water. Membranes were then incubated for 2 min with an extended range enhanced chemiluminescence reagent (WesternBright Quantum HRP; Advansta, Menlo Park, CA, USA) optimized for digital image acquisition, and then examined with a G-Box CCD imager (Syngene, Frederick, MD, USA). Unsaturated images were captured with Gene Tools imaging software for band density quantification. β-tubulin served as loading control.

2.6 Immunohistochemical analysis of nerve fibers

Figure 1 summarizes the procedure developed to analyze autonomic innervation and the colocalization of autonomic protein markers with GM-1 in sinoatrial and atrial regions.

2.6.1 GM-1 immunohistochemistry optimization—Sections (12 μm) were cut from paraffin blocks using a cryostat at −20°C, mounted onto gel coated slides with frosted ends (Electron Microscopy Sciences, Hatfield, PA, USA), air dried for 1 h, stored at −80°C, and then brought to room temperature before further processing. *In situ* GM-1 preservation was achieved by cold (−20°C) anhydrous acetone (Sigma Aldrich) fixation and permeabilization for 3 min followed by drying for 15 min in coplin jars [Heffer-Lauc et al., 2004; Heffer-Lauc et al., 2007; Petr et al., 2010; Scharwz et al., 1997]. Individual wells were formed for each section with a pap-pen (Sigma Aldrich). Sections were then blocked with ice cold PBS Plus (10 mg/mL protease-free bovine serum albumin, 5% normal goat serum, 0.01% NaN_3; Jackson ImmunoResearch, West Grove, PA, USA) for 1 h at 4°C, incubated in CtxB-594 diluted in PBS Plus for 6 h at 4°C, rinsed with cold PBS Plus 10·5 min on an orbital shaker, incubated with DAPI (1 mg/mL; Life Technologies, Carlsbad, CA, USA) in PBS for 1 min, and then sequentially rinsed with deionized water and immunofluorescence mounting solution (Electron Microscopy Sciences, Hatfield, PA, USA) before applying fresh mounting medium. Coverslips were placed and sealed with nail varnish. Sections were kept moist throughout the procedure to avoid immunofluorescence artifacts.

2.6.2 Immunohistochemistry of autonomic markers—Sections were processed as described above, and incubated overnight at 4°C with primary antibodies diluted in cold PBS Plus. Sections were rinsed with cold PBS Plus 10·5 min on an orbital shaker, and then

incubated for 3 h at 4°C with Alexafluor-488 conjugated secondary antibodies diluted in cold PBS Plus. Sections were then rinsed 4·5 min with cold PBS Plus, and sequentially incubated with 4′,6-diamidino-2-phenylindole (DAPI) in PBS, deionized water and mounting medium as described above, before applying coverslips.

2.6.3 Co-localization of GM-1 with δ-OR and autonomic markers—Color photomicrographs were acquired at constant exposure at 40X and scaled using an Olympus microscope (BX41) equipped for epifluorescence and an Olympus DP70 digital camera with DP manager software (version 2.2.1) to determine the extent of overlap of GM-1 with δ-OR and autonomic markers on neural structures within atrial tissues. To assess the overlap of GM-1 with each of the other markers the images were converted to 8-bit greyscale, and the Mander's coefficient from the JACoP plug-in ImageJ (version 1.47, NIH, Bethesda, MD) was applied. The overlap of GM-1 and synapsin on neural structures within sinoatrial tissue was also assessed from color photomicrographs obtained at 200X to more accurately determine the distribution of GM-1 within cardiac tissues.

2.6.4 Image acquisition, image reconstruction and line scan analysis—Color micrographs were captured at constant exposure and scaled using an epifluorescence microscope (100X magnification) and ImageJ software. Exposure times were adjusted to optimize signal:noise contrast. Computer images were processed with ImageJ and the Morphology plug-in. Micrographs were first converted to 8-bit greyscale images (Figure 2A) and then intensity data from the structural markers were extracted from images with uneven backgrounds using the Domes algorithm (Figure 2B). The reconstructed micrographs provided a strong first approximated background adjustment. Empirical observations demonstrated this image reconstruction algorithm generated accurate representations of the relative peak heights. Three vertical and 3 horizontal line scans, equally spaced and spanning the micrograph (Figure 2B) were then obtained and imported into MATLAB to analyze fluorescence intensities [Sathyanesan et al., 2012]. Line scan data were readjusted for baseline estimation using the "msbackadj" function, and the "preserve heights" function was used to preserve the relative sizes of peaks. Then, the "mspeak" function was applied to detect peaks. The latter command was modified to record peaks above threshold, as determined by the average peak intensity of the control line intensity scans. Line intensity scans of confocal images demonstrate that peak intensity magnitude and width are correlated with fiber size, although differentiating fibers based on peak widths obtained solely from epifluorescence images is not valid [Sathyanesan et al., 2012]. Thus, peaks in atrial and sinoatrial nodal tissue sections were assigned to bins based on fluorescence intensity, and counted digitally. Peaks were empirically assigned to intensity ranges corresponding to small fibers/neurites and larger fibers. Representative horizontal and vertical line intensity scans (Figure 2C) illustrate low intensity and high intensity peaks (Figure 2D). It was empirically determined that modifying the peak detection algorithm to correct for over-segmented peaks, i.e. repeated counting of fibers, was not necessary if the data were treated identically.

2.7 Sources of antibodies

Rabbit polyclonal antibody reactive against C-terminal δ-OR sequence was obtained from Research and Diagnostic Antibodies (Las Vegas, NV, USA). Rabbit polyclonal antibody reactive against synthetic peptide from VAChT and rabbit monoclonal antibodies reactive against synthetic peptides from ChT-1 and TH were obtained from Abcam (Cambridge, MA, USA). Rabbit monoclonal antibodies reactive against synthetic peptides from β-tubulin were acquired from Cell Signaling Technology. Cholera-toxin subunit B conjugated to Alexafluor 594 (CTxB-594) was acquired from Life Technologies (Grand Island, NY, USA) for GM-1 detection. Preabsorbed goat anti-rabbit secondary antibodies conjugated to Alexafluor 488 or horseradish peroxidase were acquired from Jackson ImmunoResearch and Cell Signaling Technology, respectively. Antibody dilutions are reported in Table 1.

2.8 Statistical analysis

Results are presented as mean values ± SEM. Immunohistochemistry data in sham and IHT animals were compared by Student's t-test for unpaired samples. Immunoblot data from the 3 groups were analyzed by single-factor ANOVA followed by Holms-Sidak's or Fishers' Least Significant Difference *post hoc* tests. P values <0.05 were taken to indicate statistically significant treatment effects. Statistical analyses were performed with SigmaStat software.

3. RESULTS

3.1 IHT-induced parasympathetic plasticity and vagal responses to nodal MEAP

Vagal stimulations were conducted to test the hypothesis that IHT augments vagal bradycardia. Resting heart rates in anesthetized dogs were not different (P=0.54) after IHT (133 ± 5) *vs* sham training (124 ± 10). Vagal transmission at 3 Hz produced a sharp decline in heart rate, the magnitude of which was appreciably greater (P<0.05) in IHT (−57 ± 6 min^{-1}) *vs.* sham trained (−37 ± 2 min^{-1}) dogs (Figure 3).

Vagal transmission was re-evaluated during the introduction of increasing doses of the δ-OR agonist MEAP into the SA node via microdialysis. Historically, nodal MEAP increases vagal transmission at low doses and suppresses it at higher doses through opposing δ_1 and δ_2-ORs [Farias et al., 2003]. In this case however, MEAP was without significant effect throughout the entire dose response (Figure 3) consistent with an already maximal δ_1-OR (vagotonic) response and an absent or minimal δ_2-OR (vagolytic) response.

3.2 IHT did not modulate peripheral δ_2-OR responses

Increasing doses of met-enkephalin were instilled into the descending aorta to evaluate the gangliolytic effect of δ_2-OR on femoral arterial blood flow. The progressive hyperemic effect was virtually identical in IHT and sham dogs (Figure 4) indicating the response of these peripheral preganglionic δ_2-OR was not altered by hypoxia training.

3.3 IHT-induced cardiac autonomic and opioidergic plasticity

The δ-OR content in the atrial lysates was similar among IHT-trained and sham animals (Figure 5A, B). When, however, the IHT protection was abrogated by daily δ-OR blockade with naltrindole, the atrial δ-OR protein expression nearly doubled *vs.* sham (P<0.05) and

IHT (Figure 5B, P<0.05)). Left ventricular lysates yielded similar results (Figure 5C) with the δ-OR content of the IHT + naltrindole group 2.9 fold that of the IHT group (P<0.01) and 2.5 fold that of the shams (P<0.01). This suggests that interrupting δ-OR signaling during hypoxia training triggers a compensatory up-regulation of myocardial δ-ORs.

A similar pattern was observed for the cholinergic marker VAChT in atria. VAChT content was not different between IHT and sham animals but daily blockade of δ-OR signaling with naltrindole during IHT provoked a compensatory 1.9-fold rise *vs.* sham (P<0.05) and 2.3-fold rise *vs.* IHT (P<0.01) (Figure 5B). This VAChT response was not observed in the ventricular extracts where vagal influences are less easily demonstrated (Figure 5C).

The ubiquitinated 70 kDa form of VAChT was also increased following opioid receptor blockade relative to IHT (Figure 5B; ANOVA, P=0.042; least squares difference *post hoc* analysis, P=0.027, IHT *vs.* IHT + naltrindole). The ratio of non-ubiquitinated (47 kDa) to ubiquitinated VAChT (70 kDa) [Li et al., 2012] was also increased following daily naltrindole (ANOVA: P=0.038; Holms-Sidak *post hoc* analysis: P= 0.046, IHT *vs.* IHT + naltrindole) suggesting that δ-OR signaling may modulate VAChT turnover. In contrast, the atrial and ventricular expression of the more widely distributed choline transporter (ChT-1) was unaltered by any of the treatments (Figure 5B, C).

No significant changes in atrial TH content were detected among the three groups (Figure 5B). Ventricular TH content declined by approximately 30% in IHT hearts but the difference fell short of statistical significance (ANOVA: P=0.066) relative to the other two groups (Figure 5C). The difference was however significant when the IHC and sham conditioned animals were compared alone (P=0.03, Student's t-test). Thus, IHT appears to facilitate a protective shift in autonomic balance.

3.4 Co-localization of GM-1, δ-OR, cholinergic, and adrenergic markers

The overlap of fluorescent CtxB-594 labeled $GM1^+$ and fluorescent antibody labeled $\delta\text{-}OR^+$, $ChAT^+$, $VAChT^+$, $ChT\text{-}1^+$, and TH^+ structures (Figure 6) was quantified by Mander's coefficients. The overlap between the labels was extensive with the $\delta\text{-}OR^+$ fibers representing 44% of the larger pool of $GM\text{-}1^+$ fibers. Conversely, 62% of the $\delta\text{-}OR^+$ fibers were also positive for GM-1 (Figure 6). For all other markers, 55%, 48%, and 35% of GM-1 fluorescence overlapped fluorescence of the cholinergic markers VAChT, ChT-1, and ChAT, respectively, and 40% of GM-1 fluorescence overlapped fluorescence of the adrenergic marker, TH. Conversely, 45%, 54% and 44% of VAChT, ChT-1 and ChAT fluorescence, respectively, overlapped GM-1 fluorescence, and 45% of TH fluorescence overlapped GM-1 fluorescence. Collectively, these results indicate that GM-1 co-localizes to a somewhat greater extent with cholinergic and $\delta\text{-}OR^+$ nerve structures than with adrenergic nerve structures. These associations are consistent with prior reports [Deo et al., 2008, Mousa et al., 2011]. Note that the overlap of GM-1 with VAChT may be underestimated due to the presence of large nerve structures in this image (Figure 6H). The overlap between GM-1 and synapsin (Figure 7) verifies the high fluorescence intensity distribution of this ganglioside within mostly neural tissues in the heart, making it useful as a structural marker for cardiac autonomic nerve fibers.

3.5 Parasympathetic remodeling in sinoatrial node and atrial myocardium

Myocardial nerve fiber distributions were evaluated from reconstructed photomicrographs with line scan intensity analyses which partitioned GM-1$^+$ fluorescent labeled fiber sizes by relative signal intensity (Figure 8A, B). When applied to the sinoatrial node, no IHT treatment effects were observed (Figure 8C, E) save for a modest upward trend in large diameter high intensity fibers (peak intensities >19; data not shown). Similarly, IHT increased the moderate intensity GM-1$^+$ fibers in the broader atrial tissue (Figure 8D), but not quite significantly (P=). However, the smaller GM-1$^+$ fibers (peak intensities 5–9) were clearly increased by IHT (P<0.05, Figure 8F). This increase in presumed neurite formation may represent early stages of structural re-arborization.

Similar line scan analyses were performed with δ-OR positive fibers most of which are presumed to be parasympathetic [Deo et al., 2008; Mousa et al., 2011]. Line scan intensity profiles of both sinoatrial and atrial δ-OR$^+$ nerves demonstrated unexpected but consistent decreases in δ-OR$^+$ structures corresponding to low intensity fibers (peak intensities 5–9) in IHT *vs.* sham dogs (P<0.05; Figure 8E, F).

Consistent with the suggestion of parasympathetic terminal outgrowth, IHT increased the number of sinoatrial nodal VAChT$^+$ fibers (Figure 8C; P<0.05 *vs.* sham). Individual analysis by fiber size in the sinoatrial node suggests this increase was primarily represented by the smaller low intensity fibers (peak intensities 5–9, P<0.05: Figure 8E). Similar but non-significant trends were observed in the atria (Figure 8D).

Line scan analyses of the more widely dispersed ChT-1 identified no IHT mediated differences in labeled fibers of any intensity in sinoatrial nodal or atria (Figure 8C–F). Similarly, line scan intensity profiles revealed no changes in TH-positive nerves in sinoatrial node following IHT, while in atria, a downward trend was apparent in both moderate and low intensity TH$^+$ fibers in IHT *vs.* sham dogs (Figure 8D, F).

Since autonomic balance is a key physiological factor, changes in the relative cholinergic and adrenergic densities were examined. Ratios of total VAChT$^+$ and ChT-1$^+$ fibers to TH$^+$ fibers at intensities >4 were computed from the data in Figure 8. A trend in favor of an improved parasympathetic influence was observed, although the compound error associated with the procedure precluded a statistically significant outcome. Additionally, the GM-1$^+$ innervations relative to the δ-opioidergic innervations determine the balance of vagotonic δ_1-OR *vs.* vagolytic-δ_2-OR. Therefore, the ratios of GM-1$^+$ to δ-OR$^+$ fibers at intensities >4 were computed. IHT appears to favor an increase in the GM-1 associated with δ-OR$^+$ labeled fibers (GM-1:δ-OR ratios: Sham 2.98 ± 0.46 *vs.* IHT 3.96 ± 0.32 SEM; P=0.13). Although again the increase is not significant due to the large variation, the upward trend is consistent with an association between rising GM-1 and functional improvements in vagal transmission.

4. DISCUSSION

4.1 Major findings

Chronic intermittent hypoxia training (IHT) produces a myocardial adaptation that affords a remarkable degree of cardioprotection following severe coronary ischemia [Zong et al., 2004]. The current analyses were undertaken to investigate further the recent findings that this protection is abrogated by coincident daily δ-OR blockade [Estrada et al., 2016]. The known cardioprotective influence associated with hypoxia-induced δ-opioid signaling [Maslov et al., 2013] and its ties to cholinergic transmission [Jackson et al., 2001; Farias et al., 2001, 2003; Deo et al., 2008; Mousa et al., 2011] led to the hypothesis that IHT would increase the efficacy of one or both of these interdependent protective systems. The goal was to demonstrate both potential functional and structural support for the hypothesis.

Intermittent hypoxia training induced a functional shift in the autonomic balance in favor of increased parasympathetic influence on the heart, manifest as an enhanced bradycardic response to external vagus nerve stimulation. Several factors may have contributed to these changes. Since the vagus was physically ligated, the pacemaker appears to have been sensitized to cholinergic stimulation. This increase in the efficacy of parasympathetic transmission is supported structurally by the rise in VAChT labeled fibers. The increase in cholinergic fibers was concentrated among the lower intensity fibers and, thus, may reflect new neurite growth. The same increase in VAChT labeled fibers was not observed for the widely distributed choline transporter suggesting further that the changes reflect a localized increase in the terminal arborization and/or the local density of varicosities.

The vagal response to intra-nodal MEAP is δ-OR subtype dependent and the integrated sum of a bimodal response [Farias et al., 2003]. At ultralow MEAP concentrations, prejunctional δ_1-OR stimulation improves vagal efficacy (vagotonic) and at higher concentrations, the more prominent δ_2-OR stimulation suppresses that same vagal transmission (vagolytic). IHT seems to have altered that pattern such that a relatively robust vagotonic response is observed throughout the dose response and the competing vagolytic response is muted or absent. This pattern would be consistent with a decline in the vagolytic δ_2-OR phenotype exposing a now unrestrained vagotonic δ_1-OR phenotype. The regular hypoxic stress associated with IHT clearly elicits daily δ-OR stimulation since δ-OR blockade prevents the evolving cardioprotection. Opioids are notorious for their ability to downregulate receptors following repeated exposure. Prior studies also indicate that repeated sublethal ischemic stress or exposure to GM-1 both result in a decline in the vagolytic δ_2-OR response [Deo et al., 2009; Davis et al., 2006]. In addition to the hypoxic stress, IHT appears to produce both an increase in GM-1 and a decline in δ-OR content. The functional, structural and biochemical findings would all be consistent if the majority of the decline in δ-OR was of the vagolytic δ_2-OR variety. In support of this thesis, GM-1 is widely associated with lipid rafts and the cyclic-AMP dependent δ_1-OR [Ledeen and Wu, 2015]. Thus, an increase in lipid rafts would also facilitate a shift in δ-ORs in favor of the vagotonic δ_1-OR phenotype. The autonomic regulation of peripheral vasoconstriction is similarly moderated by prejunctional gangliolytic δ_2-ORs [Barlow et al., 2011]. The enkephalin mediated regulation of femoral arterial conductance was virtually identical in sham and IHT groups. Thus, the

change in responses appears to be specific to the heart, which may reflect a fundamental distinction in the effect of hypoxia on resting skeletal muscle versus working cardiac muscle.

The protection afforded by IHT is supported by several key structural changes. IHT increased both the VAChT and GM-1 labeled fibers in the parasympathetically dense atria. When categorized by size, the increases were concentrated among smaller and presumably newly evolving fibers. This is logically consistent with the neurotrophic properties of GM-1 [Ledeen and Wu, 2015]. More than 90% of atrial cholinergic fibers are co-labeled as δ-OR positive [Deo et al., 2008]. There was an extensive overlap between GM-1 and δ-OR positive nerve fibers which should produce an environment conducive to the vagotonic δ_1-OR. As noted above, an increase in the GM-1 populated lipid rafts and nascent nerve growth should shift the opioid receptors in favor of the vagotonic δ_1-OR phenotype. Contrary to the original hypothesis, total δ-OR protein content and nerve fiber counts declined after IHT. This would however be completely congruent with the current functional and molecular observations if the decline in receptor labeling were primarily from the larger pool of δ_2-ORs. In support of this concept, administering GM-1 into the SA node by dialysis produced a progressive elimination of the vagolytic δ_2-OR response [Davis et al., 2006] presumably by enhancing the lipid raft environment in which the prejunctional δ-OR operates. This part of the subtype hypothesis will require pharmacologic confirmation with subtype selective antagonists [Farias et al., 2003].

The use of GM-1 as a nerve marker in heart is novel and its implications regarding nerve growth and opioid receptor function will also require further investigation. The relative increase in non-ubiquinated VAChT suggests a reduction in the turnover of this key marker and supports the concept of a dynamically adapting parasympathetic limb. The IHT mediated decline in left ventricular TH content and downward trend in TH positive fibers supports an evolving shift in myocardial autonomic balance in favor of a protective parasympathetic influence. This conclusion is further supported by observations in humans where an enhanced vagal control over the heart, accompanied by decrease tachycardic responses to hypoxia stimulus, following 14 d of intermittent hypoxia exposure was demonstrated [Zhang et al., 2014].

The remarkable cardioprotective effect of IHT reported earlier was completely abrogated by regular δ-OR-blockade with naltrindole [Estrada et al., 2016]. Even though the number of blocked subjects presented in this study is limited, the data from δ-OR-blockade are strikingly consistent. Both opioid and vagal components demonstrate sharp compensatory increases following the blockade, supporting the hypothesis that δ-OR signaling is an integral component of the evolving IHT cardiac phenotype [Zong et al., 2004; Mallet et al., 2006; Manukhina et al., 2013]. These findings provide interesting parallels to exercise training which also protects the heart with similar changes in autonomic function [Rodrigues et al., 2014].

4.2 Mechanisms underlying improved autonomic function following IHT: An evolving hypothesis

Despite its remarkable therapeutic potential and non-invasive character very little is understood about the mechanisms by which IHT protects the heart. The robust character of the protection suggests that multiple, perhaps convergent, pathways are involved [Estrada et al., 2016]. Figure 9 provides a simplified diagram of what is currently established. Intermittent hypoxic stress temporarily increases norepinephrine, enkephalin and reactive oxygen species when interleaved with sufficient periods of re-oxygenation to reestablish equilibrium. Each of these factors is necessary to produce the new cardioprotective phenotype since negating any abrogates the protection completely [Mallet et al., 2006; Estrada et al. 2016].

The evolving hypothesis suggests that all three IHT signal systems, i.e. β-adrenoreceptors, δ_1-OR and ROS, stimulate protein kinase A (PKA) activity. At this point one consequence is an increase in the PKA-dependent galactosyltransferase activity and the resulting synthesis of neurotrophic GM-1 [Ledeen and Wu, 2015]. The influence of GM-1 appears to be at least twofold. Acutely, it alters membrane lipid rafts to provide an environment that favors the cardioprotective vagotonic δ_1-OR over its opposing vagolytic δ_2-OR. One immediate consequence is better vagal transmission. Second, when GM-1 accumulates in the heart, it appears to specifically induce vagal neurite growth and presumably a more efficient vagal myocardial interface. GM-1 mediated neuritogenetic signaling cascades may also benefit from downstream interactions with PKC activity as previously proposed [Estrada et al., 2016]. However, the specific molecules involved in mediating any concerted actions of these two agents may differ within myocardial [Zong et al., 2004], endothelial [Manukhina et al., 2013], and neural [Li et al., 2016] tissues. Collectively, although vagal activity is clearly protective, this simplistic mechanism is almost surely incomplete. The interaction between the three humoral effectors must be more complex since all three are required and no partial cardioprotection was observed following individual blockade [Mallet et al., 2006; Estrada et al., 2016].

4.3 Conclusions

The extraordinary cardioprotection associated with the noninvasive application of limited daily intermittent normobaric hypoxia appears to employ a slowly evolving collection of complimentary adaptations that include favorable changes in GM-1 ganglioside synthesis, δ_1-OR expression, parasympathetic fiber arborization and ultimately better cardiac vagal transmission. This inexpensive and practical approach to cardioprotection appears to produce a whole greater than the sum of the parts. Despite the current results, more questions remain and, thus, this potentially life-saving protocol clearly warrants further careful investigation.

Abbreviations

AR	adrenergic receptor
ChT-1	choline transporter-1

IHT	intermittent hypoxia training
OR	opioid receptor
ROS	reactive oxygen species
TH	tyrosine hydroxylase
VAChT	vesicular acetylcholine transporter

References

Barlow MA, Deo SH, Caffrey JL. Sympatholytic delta-2 opioid receptors moderate ganglionic vasomotor control. Exp Biol Med (Maywood). 2011; 236:341–51. DOI: 10.1258/ebm.2011.010341 [PubMed: 21378030]

Cubillos-Rojas M, Amair-Pinedo F, Tato I, Bartrons R, Ventura F, Rosa JL. Simultaneous electrophoretic analysis of proteins of very high and low molecular mass using Tris-acetate polyacrylamide gels. Electrophoresis. 2010; 31:1318–1321. DOI: 10.1002/elps.200900657 [PubMed: 20309890]

Davis S, Deo SH, Barlow M, Yoshishige D, Farias M, Caffrey JL. The monosialosyl ganglioside GM-1 reduces the vagolytic efficacy of delta2-opioid receptor stimulation. Am J Physiol Heart Circ Physiol. 2006; 291:H2318–26. DOI: 10.1152/ajpheart.00455.2006 [PubMed: 16815987]

Deo SH, Barlow MA, Gonzalez L, Yoshishige D, Caffrey JL. Cholinergic location of delta-opioid receptors in canine atria and SA node. Am J Physiol Heart Circ Physiol. 2008; 294:H829–38. DOI: 10.1152/ajpheart.01141.2007 [PubMed: 18032518]

Deo SH, Barlow MA, Gonzalez L, Yoshishige D, Caffrey JL. Repeated arterial occlusion, delta-opioid receptor (DOR) plasticity and vagal transmission within the sinoatrial node of the anesthetized dog. Exp Biol Med (Maywood). 2009; 234:84–94. DOI: 10.3181/0808-RM-242 [PubMed: 18997098]

Estrada JA, Williams JrAG, Sun J, Gonzalez L, Downey H, Fred Caffrey JL, Mallet RT. δ-Opioid Receptor (DOR) Signaling and Reactive Oxygen Species (ROS) Mediate Intermittent Hypoxia Induced Protection of Canine Myocardium. Basic Res Cardiol. 2016; in press. doi: 10.1007/s00395-016-0538-5

Farias M, Jackson K, Stanfill A, Caffrey JL. Local opiate receptors in the sinoatrial node moderate vagal bradycardia. Auton Neurosci. 2001; 87:9–15. DOI: 10.1016/S1566-0702(00)00244-7 [PubMed: 11270142]

Farias M, Jackson K, Yoshishige D, Caffrey JL. Bimodal delta-opioid receptors regulate vagal bradycardia in canine sinoatrial node. Am J Physiol Heart Circ Physiol. 2003; 285:H1332–9. DOI: 10.1152/ajpheart.00353.2003 [PubMed: 12915393]

Heffer-Lauc M, Lauc G, Nimrichter L, Fromholt SE, Schnaar RL. Redistribution of gangliosides and glycosylphosphatidylinositol-anchored proteins in brain tissue sections under conditions of lipid raft isolation. Biochim Biophys Acta. 2004; 1686:200–208. DOI: 10.1016/j.bbalip.2004.10.002 [PubMed: 15629689]

Heffer-Lauc M, Viljetic B, Vajn K, Schnaar RL, Lauc G. Effects of detergents on the redistribution of gangliosides and GPI-anchored proteins in brain tissue sections. J Histochem Cytochem. 2007; 55:805–812. DOI: 10.1369/jhc.7A7195.2007 [PubMed: 17409378]

Jackson KE, Farias M, Stanfill AS, Caffrey JL. Transient arterial occlusion raises enkephalin in the canine sinoatrial node and improves vagal bradycardia. Auton Neurosci. 2001; 94:84–92. DOI: 10.1016/S1566-0702(01)00351-4 [PubMed: 11775711]

Kappagantula S, Andrews MR, Cheah M, Abad-Rodriguez J, Dotti CG, Fawcett JW. Neu3 sialidase mediated ganglioside conversion is necessary for axon regeneration and is blocked in CNS axons. J Neurosci. 2014; 34:2477–92. DOI: 10.1523/JNEUROSCI.4432-13.2014 [PubMed: 24523539]

Ledeen RW, Wu G. The multi-tasked life of GM1 ganglioside, a true factotum of nature. Trends Biochem Sci. 2015; 40:407–18. DOI: 10.1016/j.tibs.2015.04.005 [PubMed: 26024958]

Levy MN, Zieske H. Autonomic control of cardiac pacemaker activity and atrioventricular transmission. J Appl Physiol. 1969; 27:465–70. [PubMed: 5822553]

Li L, Tian J, Long MK-W, Chen Y, Lu J, Zhou C. Protection against Experimental Stroke by Ganglioside GM1 Is Associated with the Inhibition of Autophagy. PLoS One. 2016; 11(1):e0144219.doi: 10.1371/journal.pone.0144219 [PubMed: 26751695]

Li Y, Freeling J, Sample A. Ubiquitination of Vesicular Acetylcholine Transporter. The FASEB Journal. 2012; 26:1067–6.

Mallet RT, Ryou MG, Williams AG Jr, Howard L, Downey HF. β_1-adrenergic receptor antagonism abrogates cardioprotective effects of intermittent hypoxia. Basic Res Cardiol. 2006; 101:436–446. DOI: 10.1007/s00395-006-0599-y [PubMed: 16705468]

Manukhina EB, Belkina LM, Terekhina OL, Abramochkin DV, Smirnova EA, Budanova OP, Mallet RT, Downey HF. Normobaric, intermittent hypoxia conditioning is cardio- and vasoprotective in rats. Exp Biol Med (Maywood). 2013; 238:1413–1420. DOI: 10.1177/1535370213508718 [PubMed: 24189016]

Manukhina EB, Downey HF, Mallet RT. Role of nitric oxide in cardiovascular adaptation to intermittent hypoxia. Exp Biol Med (Maywood) 2006. 2006; 231:343–65.

Maslov LN, Naryzhnaia NV, Tsibulnikov SY, Kolar F, Zhang Y, Wang H, Gusakova AM, Lishmanov YB. Role of endogenous opioid peptides in the infarct size-limiting effect of adaptation to chronic continuous hypoxia. Life Sci. 2013; 93:373–379. DOI: 10.1016/j.lfs.2013.07.018 [PubMed: 23891777]

Mousa SA, Shaqura M, Schäper J, Treskatsch S, Habazettl H, Schäfer M, Abdul-Khaliq H. Developmental expression of δ-opioid receptors during maturation of the parasympathetic, sympathetic, and sensory innervations of the neonatal heart: early targets for opioid regulation of autonomic control. J Comp Neurol. 2011; 519:957–71. DOI: 10.1002/cne.22560 [PubMed: 21280046]

Narita M, Kuzumaki N, Miyatake M, Sato F, Wachi H, Seyama Y, Suzuki T. Role of delta-opioid receptor function in neurogenesis and neuroprotection. Neurochem. 2006; 97:1494–505. DOI: 10.1111/j.1471-4159.2006.03849.x

Petr T, Smíd V, Smídová J, Hůlková H, Jirkosvká M, Elleder M, Muchová L, Vitek L, Smíd F. Histochemical detection of GM1 ganglioside using cholera toxin-B subunit. Evaluation of critical factors optimal for in situ detection with special emphasis to acetone pre-extraction. Eur J Histochem. 2010; 54:e23d.doi: 10.4081/ejh.2010.e23 [PubMed: 20558344]

Rodrigues F, Feriani DJ, Barboza CA, Abssamra ME, Rocha LY, Carrozi NM, Mostarda C, Figueroa D, Souza GI, De Angelis K, Irigoyen MC, Rodrigues B. Cardioprotection afforded by exercise training to myocardial infarction is associated with autonomic function improvement. BMC Cardiovasc Disord. 2014; 14:84d.doi: 10.1186/1471-2261-14-84 [PubMed: 25022361]

Sathyanesan A, Ogura T, Lin W. Automated measurement of nerve fiber density using line intensity scan analysis. J Neurosci Methods. 2012; 206:165–175. DOI: 10.1016/j.jneumeth.2012.02.019 [PubMed: 22613744]

Schwarz A, Futerman AH. Determination of the localization of gangliosides using anti ganglioside antibodies: comparison of fixation methods. J Histochem Cytochem. 1997; 45:611–618. DOI: 10.1177/002215549704500413 [PubMed: 9111239]

Towbin H. Origins of protein blotting. Methods Mol Biol. 2009; 536:1–3. DOI: 10.1007/978-1-4939-2694-7_2 [PubMed: 19378038]

von Ziegler LM, Saab BJ, Mansuy IM. A simple and fast method for tissue cryohomogenization enabling multifarious molecular extraction. J Neurosci Methods. 2013; 216:137–141. DOI: 10.1016/j.jneumeth.2013.03.005 [PubMed: 23541735]

Zhang P, Downey HF, Chen S, Shi X. Two-week normobaric intermittent hypoxia exposures enhance oxyhemoglobin equilibrium and cardiac responses during hypoxemia. Am J Physiol Regul Integr Comp Physiol. 2014; 307:R721–30. DOI: 10.1152/ajpregu.00191.2014 [PubMed: 25056104]

Zong P, Setty S, Sun W, Martinez R, Tune JD, Ehrenbourg IV, Tkatchouk EN, Mallet RT, Downey HF. Intermittent hypoxic training protects canine myocardium from infarction. Exp Biol Med. 2004; 229:806–812.

Highlights

- IHT induced cardioprotection is associated with an improved autonomic profile.
- IHT augments vagally mediated bradycardia.
- Vagotonic δ_1-OR activity is enhanced by IHT at the expense of competing vagolytic δ_2-OR activity.
- IHT induces parasympathetic nerve growth in myocardium.
- Adrenergic influence over the heart is attenuated by IHT.

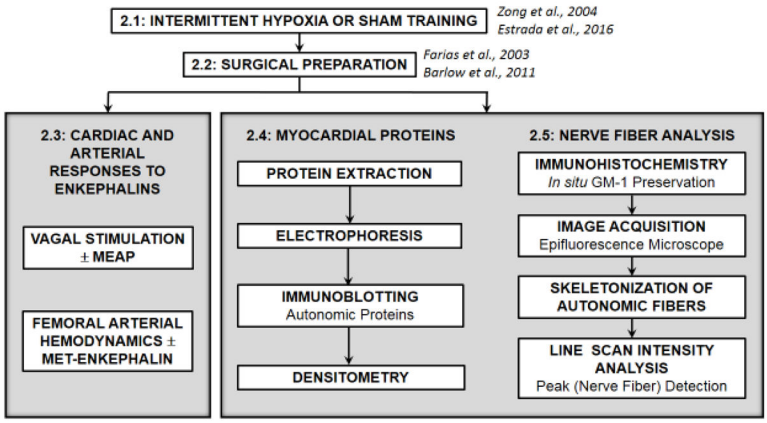

Figure 1.

Summary of experimental design, including assessments of cardiac and femoral arterial enkephalin responses, myocardial protein contents and autonomic innervation in IHT and sham-trained dogs.

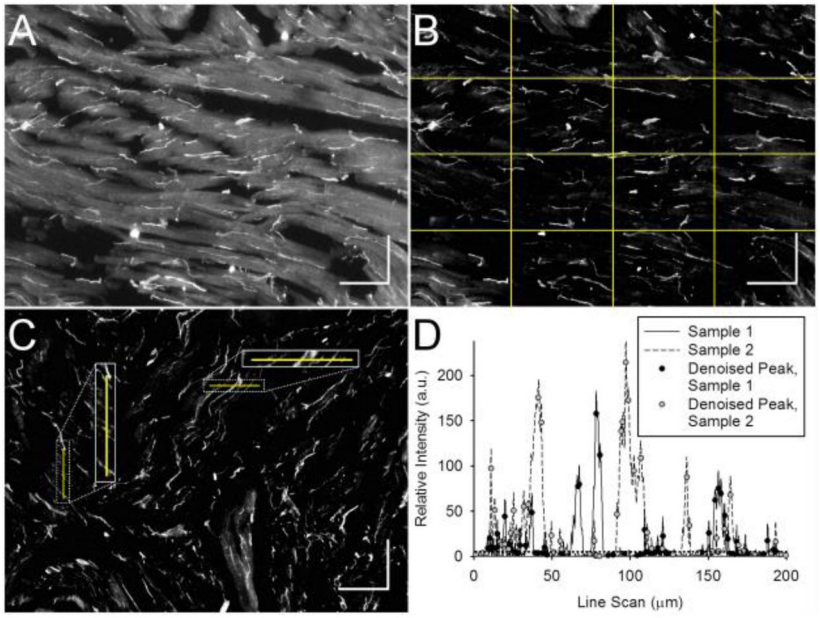

Figure 2.

Optimized GM-1 immunohistochemistry demonstrating line scan intensity data acquisition, and nerve fiber analysis. (A–C) Nerve fibers are labeled by CTxB-594 (GM-1). (A) Atrial GM-1 nerve fiber labeling followed by (B) image reconstruction with horizontal and vertical line scan overlay. (C) Sinoatrial GM-1^{+} nerve fiber labeling and image reconstruction. Image insets are scaled by a factor of 2 to highlight the sampling of nerve fibers by line scans. (D) The sample line scan intensity profiles (Sample 1: vertical; sample 2: horizontal) are subject to peak/fiber analysis in MATLAB. The denoised peaks (dark and grey filled circles) at and above background noise (5 a.u. dashed line) represent nerve fibers. Scale bars: 200 μm.

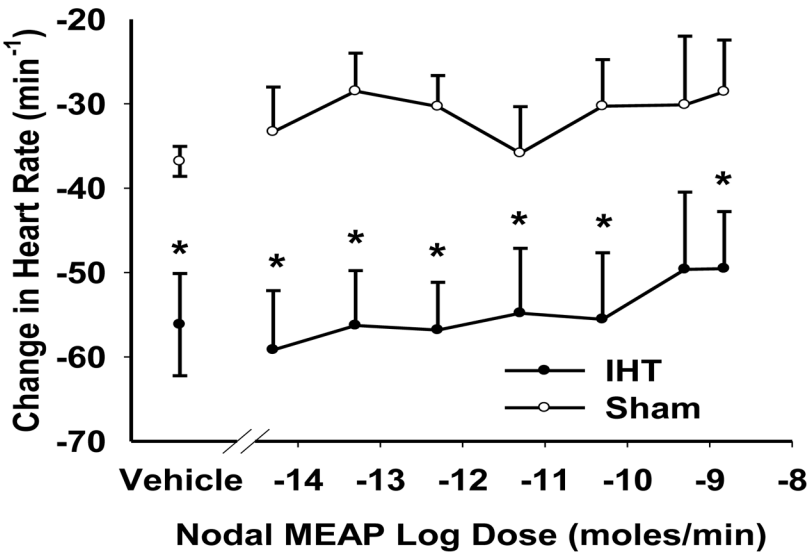

Figure 3.

Heart rate responses to vagal stimulation vs. local SA nodal met-enkephalin-arg-phe (MEAP) dose. The vagus was stimulated at 3 Hz. Values are mean ± SEM from 6 sham (open circles) and 11 IHT (filled circles) dogs. *P>0.05 *vs.* respective sham value. Pre-stimulation heart rates (min^{-1}) were not significantly different in IHT (133 ± 5) vs. sham (124 ± 10) dogs.

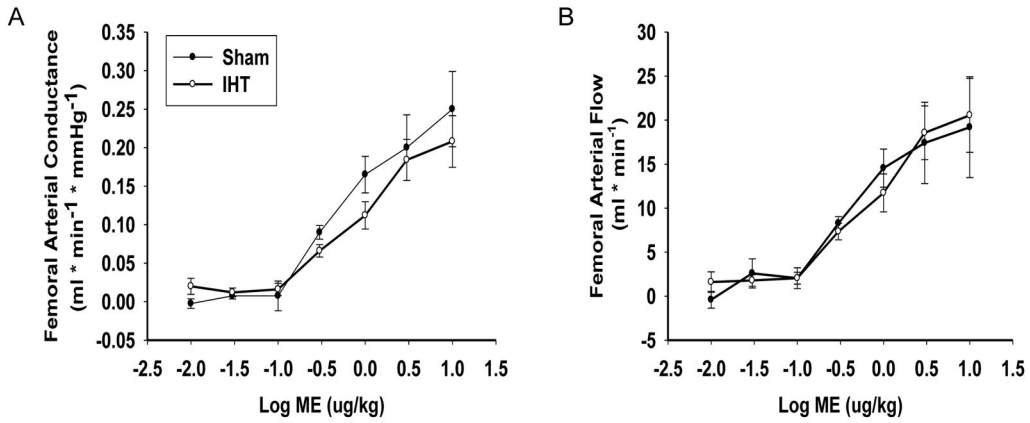

Figure 4.

Femoral arterial conductance (A) and flow (B) vs. met-enkephalin (ME) dose. Mean values ± SEM from 6 sham (filled circles) and 11 IHT dogs (open circles).

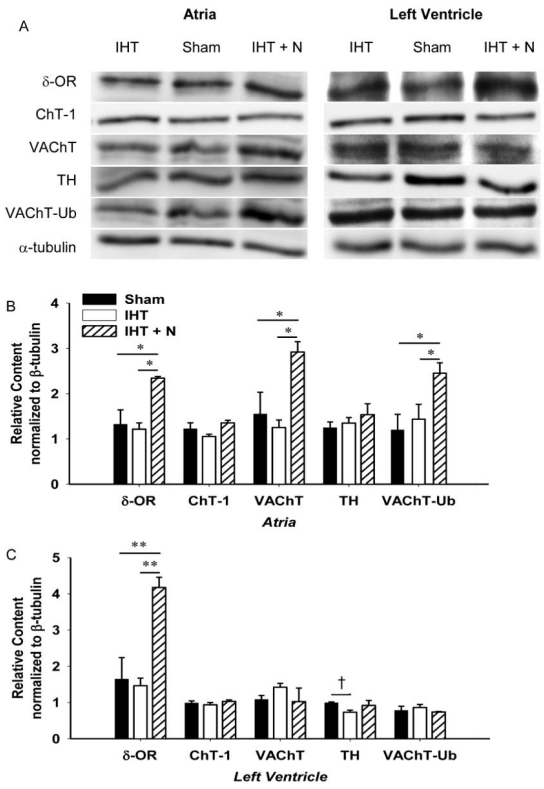

Figure 5.

δ-OR and autonomic marker contents in atrial and left ventricular myocardium. Panel A: Representative immunoblots (5–10 μg total protein/lane) of atrial and left ventricular lysates from sham trained, IHT, and IHT + N experiments. Analyte band densities (mean values ± SEM) from atria (Panel B) and left ventricle (Panel C) of 3 sham, 7 IHT and 2 IHT + naltrindole dogs. Panel B: δ-OR, VAChT and the ratio of ubiquitinated VAChT (VAChT-Ub) to VAChT are increased by IHT + N relative to IHT or sham training. Panel C: δ-OR is increased by IHT + N relative to IHT and sham training. TH is decreased by IHT relative to sham training. Values were adjusted for loading using β-tubulin. ChT-1: choline transporter-1; δ-OR: delta opioid receptor; TH: tyrosine hydroxylase; IHT: intermittent hypoxia training; IHT + N: intermittent hypoxia training + naltrindole; VAChT: vesicular acetylcholine transporter; VAChT-Ub: 70kDa ubiquitinated VAChT/VAChT. Legend, black bars represent sham training treatment, white bars IHT treatment, and hatched bars IHT + N treatment. $^{*}P<0.05$, $^{**}P<0.01$ (Holms-Sidak posthoc analysis). $^{\dagger}P<0.05$ (Student's *t*-test).

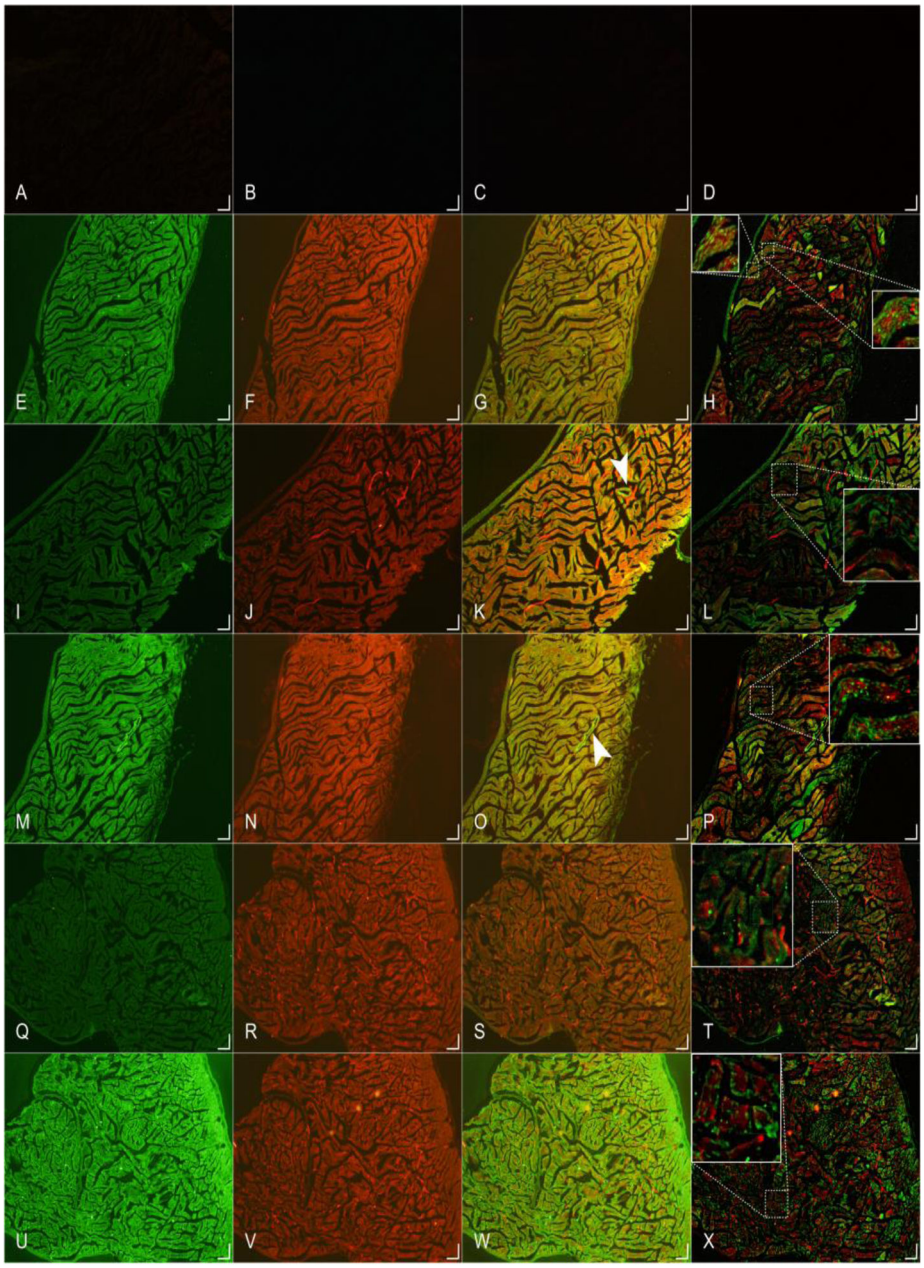

Figure 6. Colocalization of GM-1 with cardiac autonomic nerve markers in atrium

Dual immunolabelling in atrial tissue sections was used to determine the colocalization (yellow) of CTxB-594/GM-1 (F, J, N, R, V) labeled nerve fibers (red channel) with parasympathetic (E: ChAT; I: VAChT; M: ChT-1); sympathetic (Q: TH); and delta opioid receptor (U) -positive nerve fibers (green channel). Normal rabbit-sera used on control tissue sections (A, B) were negative for signal. Superimpositions (C, G, K, O, S, W) of the green and red channels created for each pair of markers illustrate their overlap. Superimpositions following skeletonization of nerve fibers (D, H, L, P, T, X) from the green and red channels illustrate nerve densities in a low autofluorescence background. Notched arrowheads

(magenta) highlight vessels co-labeled with GM1/VAChT (K) and GM1/ChT-1 (O). Horizontal and vertical scale bars are 225 μm.

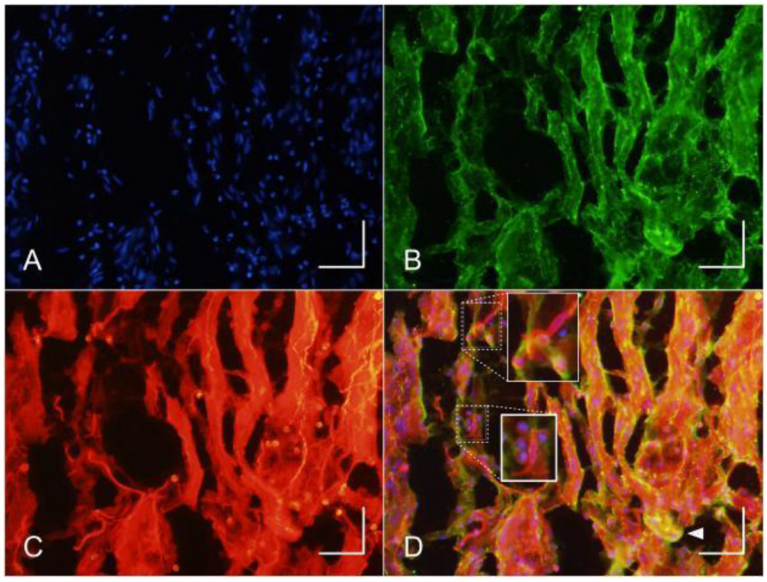

Figure 7.

Colocalization of GM-1 with synapsin in the sinoatrial node. Tissue section images were acquired at 200X following labeling with (A) DAPI, (B) anti-Synapsin-1, and (C) CTxB-594 conjugate. (D) A composite of the images demonstrates extensive overlap (yellow) of GM-1 and synapsin. Insets highlight sinoatrial nodal cells labeled by CTxB-594 and overlap of GM-1 with cell nuclei (magenta). Synapsin accumulates on the outer edges of cell bodies, as well as along the axon and nerve endings. Arrowhead (D) highlights vessel positive for GM-1:Synapsin co-labeling. Horizontal and vertical scale bars are 100 μm.

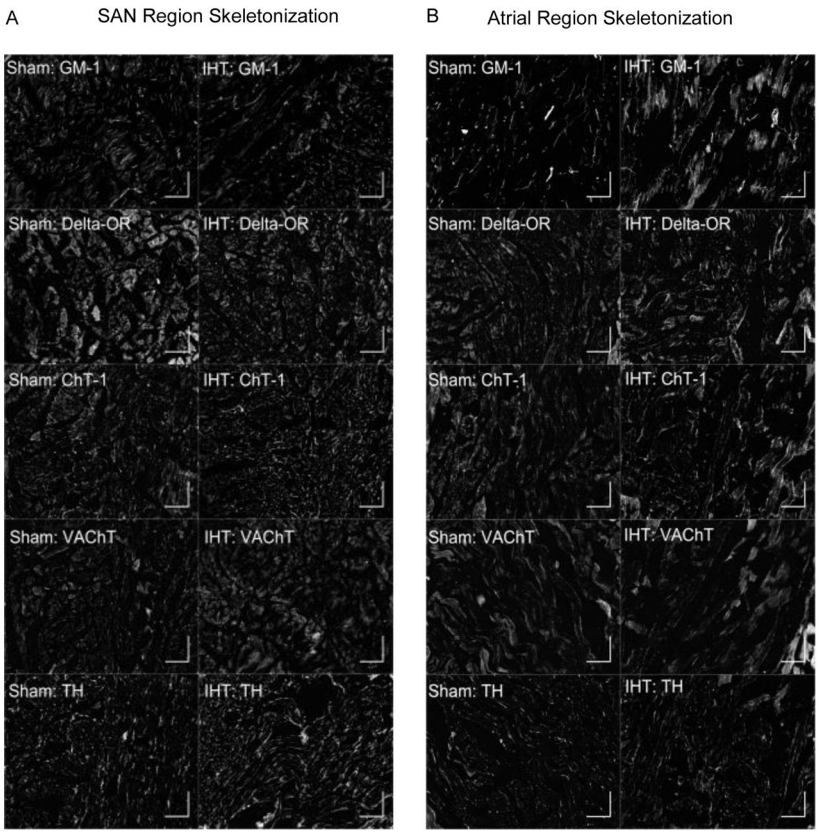

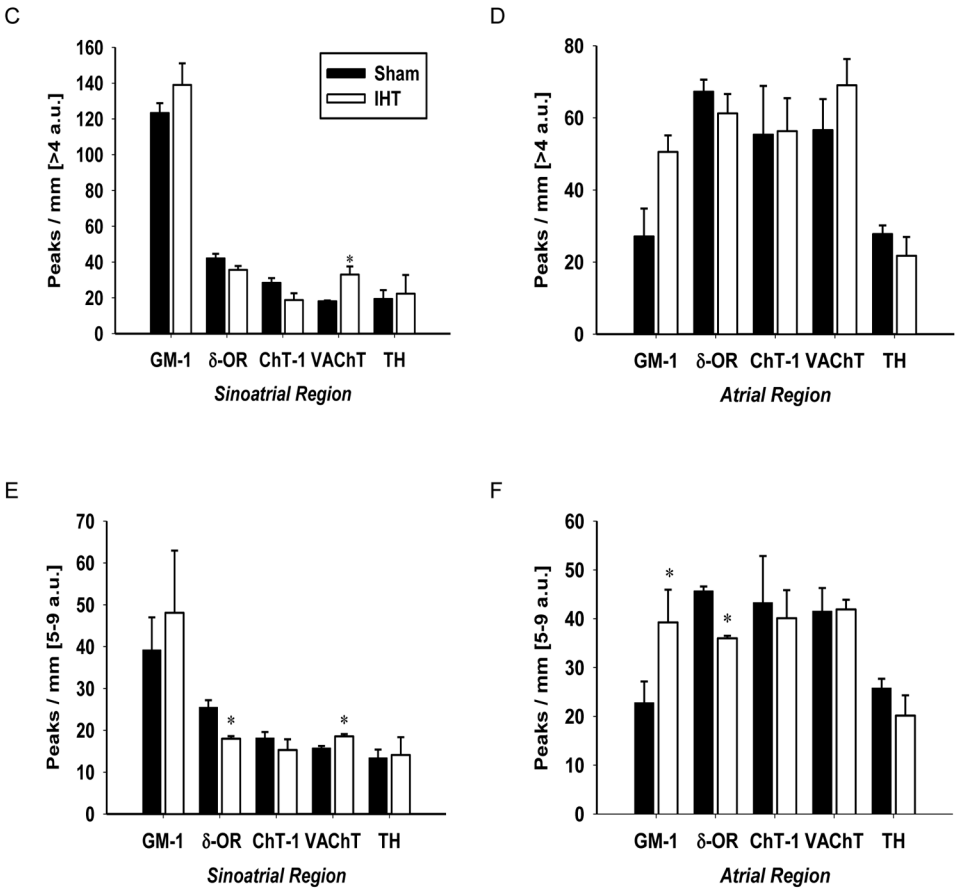

Figure 8.

Intermittent hypoxia training-induced structural remodeling of autonomic nerve fibers. Panels A and B: Markers of autonomic innervation following IHT and sham training in sinoatrial nodal (SAN; panel A) and atrial (panel B) regions after photomicrograph reconstruction. Horizontal and vertical scale bars are 200 μm. Panels C and D: Total innervations (peak fluorescence intensities greater than 4 a.u.) in the sinoatrial and atrial regions. The total parasympathetic innervation as measured by VAChT-positive peaks is increased by IHT. Panels E and F: Low intensity innervations in the sinoatrial region. Parasympathetic arborization (VAChT peak intensities of 5–9) are increased by IHT, while DOR-positive peaks in the intensity range of 5–9 are decreased by IHT. Panel F: Low intensity innervations in the atrial region. IHT increases GM-1-positive peaks in the intensity range of [5–9]. DOR-positive peaks in the intensity range of [5–9] are decreased by IHT. ChT-1: choline transporter-1; DOR: delta opioid receptor; IHT: intermittent hypoxia training; TH: tyrosine hydroxylase; VAChT: vesicular acetylcholine transporter. Filled bars: sham trained; open bars: IHT. Peaks per millimeter (mm) correspond to fiber counts. Mean values ± SEM. *P > 0.05 vs. sham trained. Sham trained, n=3 sinoatrial and atrial samples; IHT, n=5 sinoatrial and 4 atrial samples.

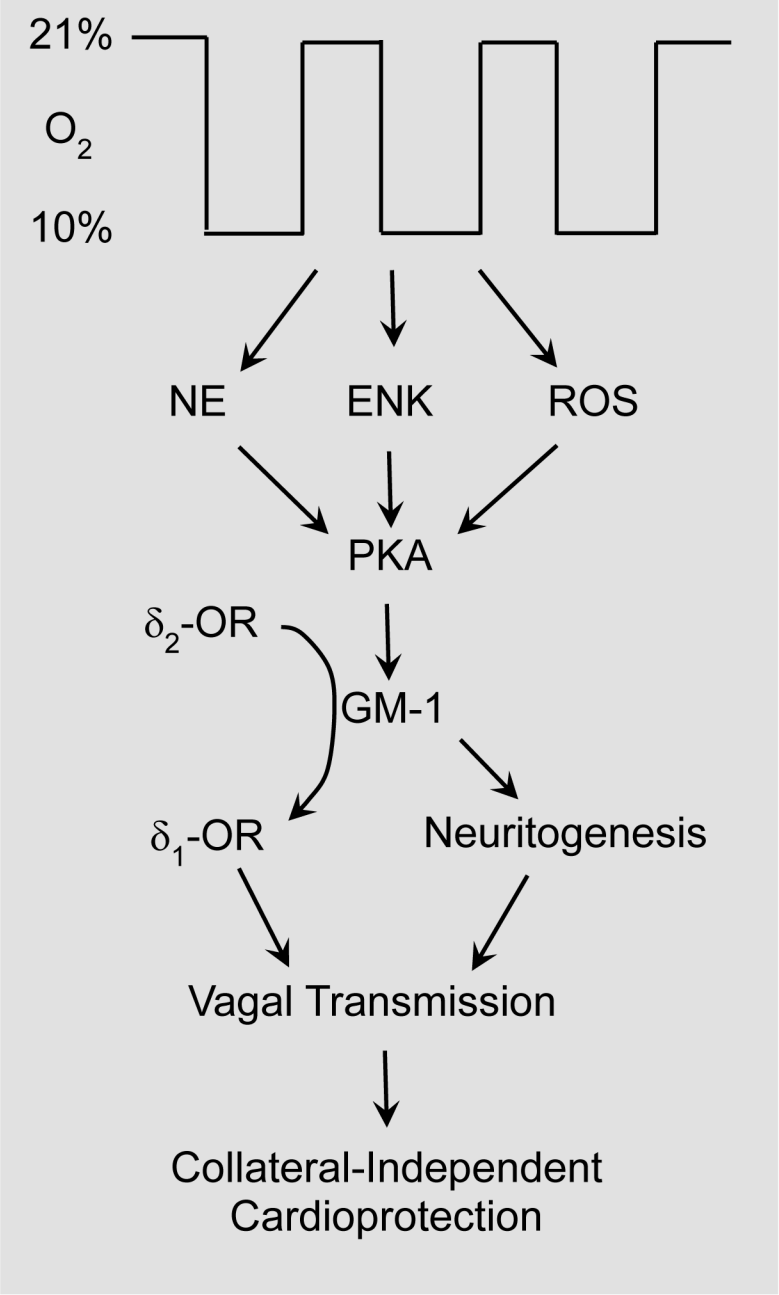

Figure 9.

Proposed model of IHT mechanisms for enhancement of autonomic function. Twenty days of intermittent hypoxia enhances autonomic function in dogs and rats. Chemoreceptors respond to hypoxia by increasing sympathetic and parasympathetic tone. Intervening cyclic-reoxygenations during hypoxia induce myocardial mitochondrial reactive oxygen species (ROS) generation, PKA activity, and PKC translocation and subsequent activation. IHT mediated increases in enkephalins (ENK) and norepinephrine (NE) stimulate δ_1-OR and β_1-AR, respectively and again PKA activity. Increased pre-synaptic PKA activity enhances vagal transmission directly and indirectly. Cyclic-AMP improves acetylcholine release and

PKA enables the positive feedback loop whereby increased GM-1 synthesis favors δ_1-OR signaling which in turn stimulates more PKA activity. The accumulated neurotrophic GM-1 facilitates synaptic plasticity and parasympathetic arborization. The net effect is enhanced parasympathetic control over the heart. The improvements in cardiac autonomic function are associated with cardioprotection against ischemia and reperfusion injury, independent of tissue salvaging collateral blood flow. $\delta_{1/2}$-OR: δ-1/2 opioid receptor.

Table 1

Antibody dilutions.

	Immunohistochemistry		Immunoblot	
	Primary	**Secondary**	**Primary**	**Secondary**
CtxB-594	1:100	-	-	-
anti Syn-1 *	1:1,000	1:100	-	-
anti ChAT *	1:100	1:100	-	-
anti TH *	1:200	1:400	1:2,000	1:10,000
anti δ-OR †	1:1,000	1:400	1:2,000	1:10,000
anti VAChT †	1:400	1:400	1:2,000	1:10,000
anti ChT-1 *	1:200	1:400	1:2,000	1:10,000
anti β-tubulin-HRP *	-	-	1:1,000	-

CtxB-594: cholera toxin subunit B Alexafluor-594 conjugate; Syn-1, synapsin; ChAT, choline acetyltransferase; TH: tyrosine hydroxylase; δ-OR: delta opioid receptor; VAChT: vesicular acetylcholine transporter; ChT-1: choline transporter-1; β-tubulin-HRP: beta-tubulin horseradish peroxidase conjugate;

* high affinity (K_D 10^{-10} – 10^{-13} M) rabbit monoclonal antibody;

† rabbit polyclonal antibody.

Highly cross-absorbed goat anti-rabbit conjugated to Alexafluor 488 and goat anti-rabbit conjugated to horseradish peroxidase were used as the secondary antibodies for all immunohistochemistry and immunoblotting experiments, respectively.